

Article

3D-QSAR Studies of Dihydropyrazole and Dihydropyrrole Derivatives as Inhibitors of Human Mitotic Kinesin Eg5 Based on Molecular Docking

Xingyan Luo, Mao Shu *, Yuanqiang Wang, Jin Liu, Wenjuan Yang and Zhihua Lin *

School of Pharmacy and Bioengineering, Chongqing University of Technology, Chongqing 400054, China

* Authors to whom correspondence should be addressed; E-Mails: sm7507@126.com (M.S.); zhlin@cqut.edu.cn (Z.L.); Tel.: +86-23-6256-3182; Fax: +86-23-6256-3182.

Received: 7 February 2012; in revised form: 7 February 2012 / Accepted: 13 February 2012 / Published: 17 February 2012

Abstract: Human mitotic kinesin Eg5 plays an essential role in mitoses and is an interesting drug target against cancer. To find the correlation between Eg5 and its inhibitors, structure-based 3D-quantitative structure–activity relationship (QSAR) studies were performed on a series of dihydropyrazole and dihydropyrrole derivatives using comparative molecular field analysis (CoMFA) and comparative molecular similarity indices analysis (CoMSIA) methods. Based on the LigandFit docking results, predictive 3D-QSAR models were established, with cross-validated coefficient values (q^2) up to 0.798 for CoMFA and 0.848 for CoMSIA, respectively. Furthermore, the CoMFA and CoMSIA models were mapped back to the binding sites of Eg5, which could provide a better understanding of vital interactions between the inhibitors and the kinase. Ligands binding in hydrophobic part of the inhibitor-binding pocket were found to be crucial for potent ligand binding and kinases selectivity. The analyses may be used to design more potent EG5 inhibitors and predict their activities prior to synthesis.

Keywords: Eg5 inhibitors; LigandFit docking; 3D-QSAR

1. Introduction

The human mitotic kinesin Eg5 is one member of the Kinesin-5 subfamily, which function is helping the formation of bipolar mitotic spindle, and has been identified as a potential target for new drug development in cancer chemotherapy [1]. Many researches had been performed to discover new

inhibition mechanismS of Eg5, such as RNA interference [2], potential inhibitors, like monoastral, which produces cells arrested in mitosis with a characteristic monoastral spindle phenotype [1,3–9]. As multidrug resistance (MDR) of anticancer drug like taxanes and vinca alkaloids has become a serious problem in cancer chemotherapy [10,11], the Eg5 inhibitors have been tested for their susceptibility to the Pgp efflux pump and some of them have been validated for greater potential to overcome MDR [12]. Thus, Eg5 inhibitors have been discovered for potential anticancer drugs [13–15].

Merck Research Laboratories scientists have reported dihydropyrazole and dihydropyrrole inhibitors with inhibitory bioactivity against Eg5 in the low nanomolar IC₅₀ range (from 1.2 nM to 829 nM) [16–18]. The compounds were used under the same conditions of an *in vitro* screening procedure based on the inhibition of the ATP kinase activity of Eg5, which like STLC leads to mitotic arrest by slowing ADP release from the catalytic site of Eg5 so that induces cancer cell death by the apoptotic pathway [19]. Some of these inhibitors showed good potency in Pgp-overexpressing cells. Thus dihydropyrazole and dihydropyrrole derivatives were described as Eg5 inhibitors that possess good to excellent intrinsic potency, aqueous solubility, low MDR ratios, limited hERG affinity, and excellent *in vivo* ability [18]. Meanwhile, Kaan *et al.* determined the crystal structure of the Eg5-STLC complex (PDB: 2WOG) [20], and reported that the inhibitive mechanism involved the fact that loop L5 of the final inhibitor-bound state was swung downwards to close the inhibitor-binding pocket, its helix $\alpha 4$ has rotated by approx 15° and the neck-linker has adopted a docked conformation. There have some articles that have adopted computer aided drug design to find new kinds of inhibitors of Eg5, but they just explored the structure-activity relationships (SAR), not the QSAR of Eg5-inhibitors [12,19,21–23]. In this paper, we examine the three dimensional quantitative structure-activity relationships (3D-QSAR) using comparative molecular field analysis (CoMFA), comparative molecular similarity indices analysis (CoMSIA) [24–30] and molecular docking (LigandFit Docking [31]) analyses, that provide insights into the relationship between the structural information of dihydropyrazole and dihydropyrrole inhibitors and their inhibitory potency, aimed at providing valuable guidance for the design of EG5 inhibitor compounds with highly anticancer activity.

2. Materials and Methods

2.1. Data Set

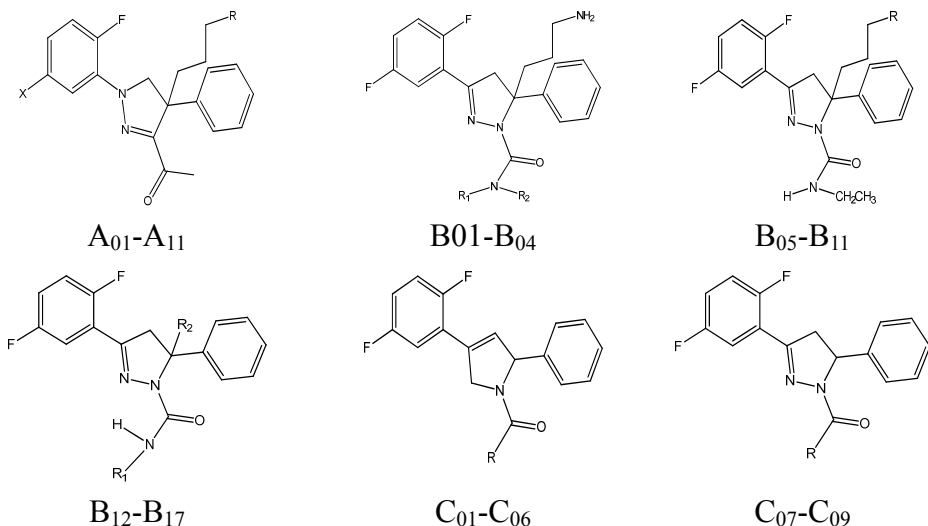
Thirty-seven dihydropyrazoles and dihydropyrroles derivatives were collected from Merck publications [16–18]. The biological data was represented as pIC₅₀. It's important to select training data and molecular alignment rules for building a good 3D-QSAR model [32] The structures of all compounds were download from the binding database [33]. The biological data was considered comparable and randomly divided into a training set (30 compounds) and a test set (seven compounds, mark with “*”), as shown in Table 1.

2.2. Molecular Docking

Molecular docking studies was performed using the LigandFit Docking module in the Receptor-Ligand Interaction package of the Accelrys Discovery Studio 2.5 software [31]. Atomic coordinates for the EG5 complex with STLC, used for docking modeling, have been deposited in the Protein

DataBank (PDB code: 2WOG) [20], the original ligand was removed from the coordinated set. All chemical compounds and their possible poses were evaluated by scoring functions.

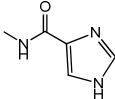
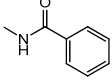
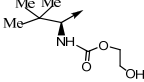
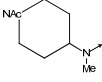
Table 1. The molecular structures and inhibitory activity of Eg5 inhibitors.



The figure shows six groups of chemical structures for Eg5 inhibitors. Group A01-A11 features a benzimidazole core with a fluorinated phenyl ring (X), a benzyl group (R), and an acetyl group. Group B01-B04 has a benzimidazole core with a fluorinated phenyl ring, a benzylamine group (NH2), and a secondary amide (R1, R2). Group B05-B11 has a benzimidazole core with a fluorinated phenyl ring, a benzyl group (R), and a primary amide (H, CH2CH3). Group B12-B17 has a benzimidazole core with a fluorinated phenyl ring, a phenyl group (R2), and a secondary amide (R1). Group C01-C06 has a benzimidazole core with a fluorinated phenyl ring and a phenyl group (R). Group C07-C09 has a benzimidazole core with a fluorinated phenyl ring and a phenyl group (R).

NO.	X	R/R ₁	R ₂	IC ₅₀ (nM)	pIC ₅₀
A ₀₁	F		-	1.2	8.9208
A ₀₂ *	CF ₃		-	2.0	8.699
A ₀₃	F		-	2.1	8.6778
A ₀₄	F		-	3.8	8.4202
A ₀₅ *	F		-	3.8	8.4202
A ₀₆	Cl		-	3.9	8.4089
A ₀₇	F		-	4.0	8.3979
A ₀₈	F		-	4.2	8.3768
A ₀₉	Br		-	4.7	8.3279
A ₁₀ *	F		-	5.2	8.284
A ₁₁	CF ₃		-	10.1	7.9957
B ₀₁	F	-(CH ₂) ₄ -	-	26.0	7.585027
B ₀₂ *	F	-(CH ₂) ₃ -	-	55.0	7.259637
B ₀₃	F	-(CH ₂) ₅ -	-	85.0	7.070581
B ₀₄	F	-(CH ₂) ₂ O(CH ₂) ₂ -	-	122.0	6.91364
B ₀₅	F	-NHBn	-	100.0	7
B ₀₆	F	-NMe ₂	-	103.0	6.9872
B ₀₇	F		-	119.0	6.9245
B ₀₈ *	F		-	391.0	6.4078
B ₀₉	F	-NMe ₂ O	-	585.0	6.2328

Table 1. Cont.

NO.	X	R\R1	R2	IC50 (nM)	pIC50
B ₁₀	F		-	686.0	6.1637
B ₁₁	F		-	829.0	6.0814
B ₁₂	F	CH ₂ CH ₃	(CH ₂) ₃ NH ₂	44.0	7.3565
B ₁₃	F	CH ₂ CH ₃	(CH ₂) ₄ NH ₂	67.0	7.1739
B ₁₄	F	CH ₃	CH ₃	284.0	6.5467
B ₁₅	F	CH ₂ CH ₃	(CH ₂) ₂ NH ₂	390.0	6.4089
B ₁₆ *	F	CH ₂ CH ₃	(CH ₂) ₄ OH	697.0	6.1568
B ₁₇	F	CH ₂ CH ₃	(CH ₂) ₃ OH	745.0	6.1278
C ₀₁	F		-	5.2	8.284
C ₀₂	F		-	7.4	8.1308
C ₀₃ *	F		-	11.0	7.9586
C ₀₄	F		-	16.0	7.7959
C ₀₅	F	NMe ₂	-	38.0	7.4202
C ₀₆	F		-	50.0	7.301
C ₀₇	F	NMe ₂	-	84.0	7.075721
C ₀₈	F	Me	-	94.0	7.026872
C ₀₉	F	t-Bu	-	113.0	6.946922

* Stands for molecules belonging to the test set (seven compounds).

2.3. 3D-QSAR Modeling [25,26]

3D-QSAR models were constructed by using CoMFA and CoMSIA in the SYBYL program package. Parameters of CoMFA and CoMSIA were the default values. The cut off value was set 30 kcal/mol. With standard options for scaling of variables, the regression analysis was performed using the “leave-one-out” cross-validation partial least squares method. The final non-cross-validated model was developed with a no validation PLS analysis.

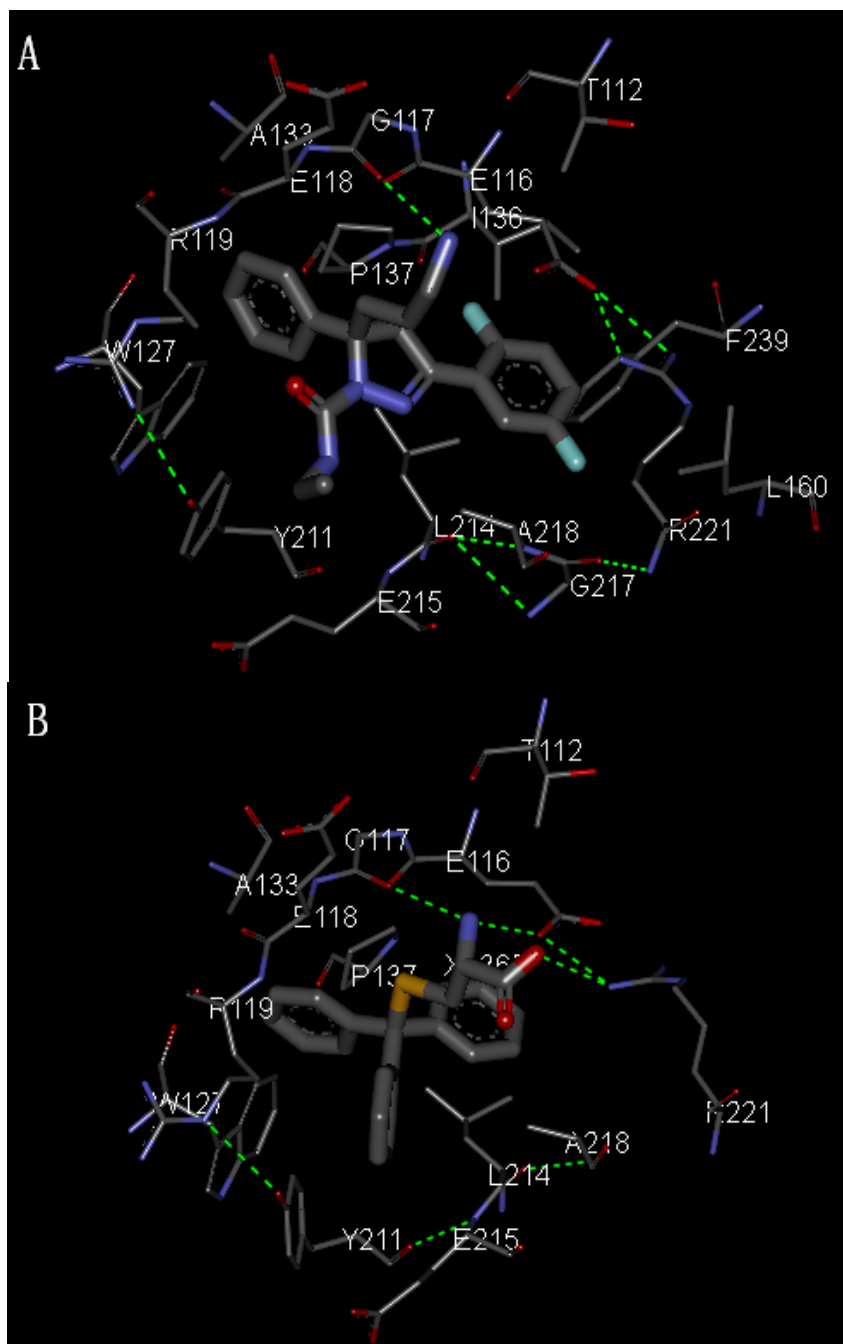
3. Results and Discussion

3.1. Molecular Docking

The molecular modeling results using a molecular docking method revealed the possible molecular orientation of STLC and the derivatives in the binding pocket of Eg5 (Figure 1). STLC and B12 were buried in the pocket by the E116, E117, E118, R119 *etc.*, and it was considered that they shared the same binding site. This suggests a similar binding mode for the dihydropyrazoles, dihydropyrroles and the

S-trityl-L-cysteine (STLC), and those compounds can arrest cells in mitosis with a characteristic monoastal phenotype [12,20].

Figure 1. (A) Eg5 X-ray structure of the allosteric binding site with the B₁₂ inhibitors in the binding site (PDB: 2G1Q); (B) Stereo plot showing STLC in the binding site (PDB: 2WOG).



Figures 2A,B show how the substituted 4, 5-dihydropyrazole derivate (*A*₀₁) is buried in the binding pocket of Glu116, Gly117, and Glu118, while the R group is in the solvent-exposed region of the protein. Ligands binding in hydrophobic part of the inhibitor-binding pocket were found to be crucial for potent ligand binding and kinase selectivity. Further QSAR analysis was obtained by optimal

conformation of inhibitors based on the LigandFit docking results. The optimal conformation of the 37 inhibitors is shown in the Figure 2C.

Figure 2. (A) Surface diagram showing the positions of the 1,4-diaryl-4,5-dihydropyrazole (A_{01}) in the pocket (PDB code: 2WOG); (B) Stereo plot showing 1,4-diaryl-4,5-dihydropyrazole (A_{01}) in the pocket (PDB code: 2WOG); (C) Overall of alignment of the 37 inhibitors obtained by the molecular docking.

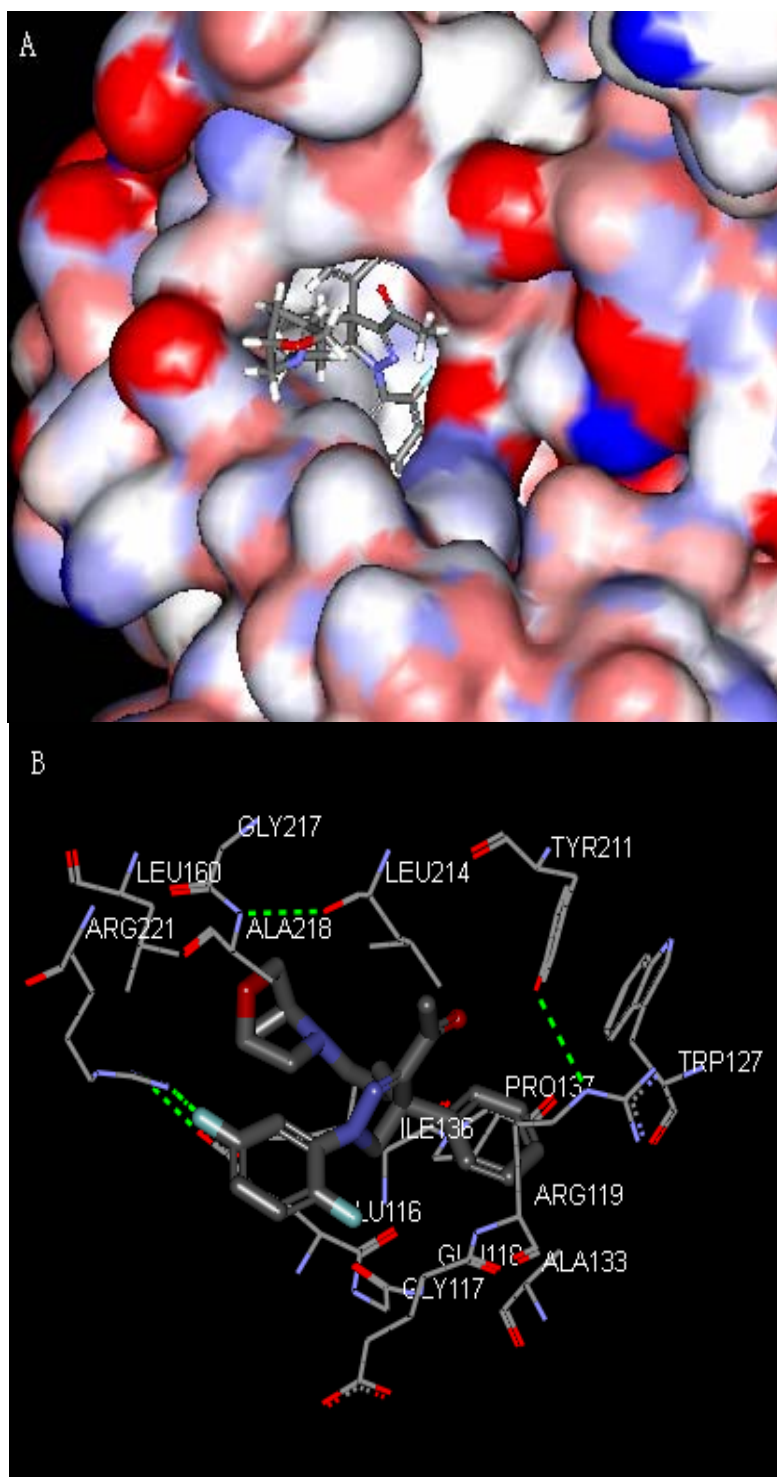
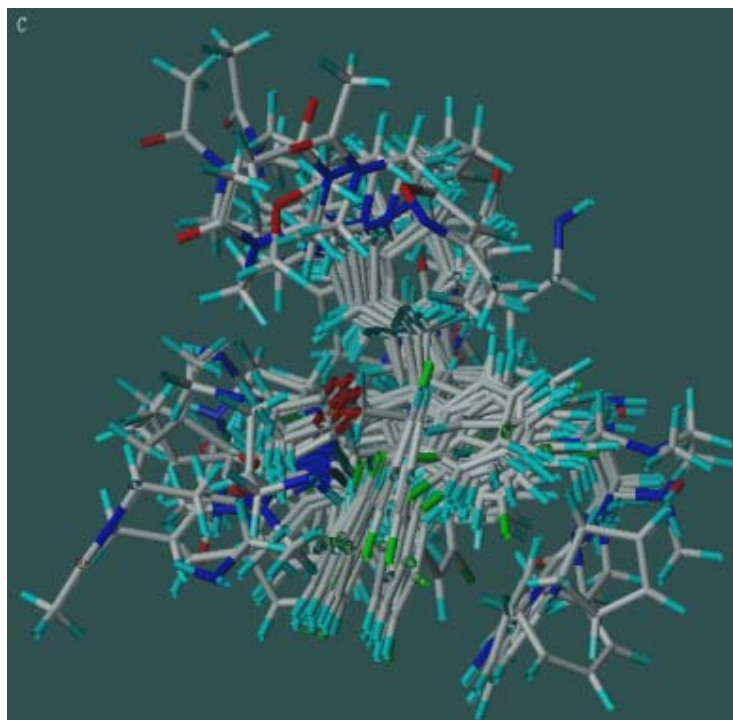


Figure 2. Cont.



3.2. CoMFA and CoMSIA of 3D-QASR Models

The results of the CoMFA and CoMSIA methods are summarized in Table 2. In the CoMFA model the cross-validated coefficient q^2 is 0.798, regression coefficient r^2 is 0.980, and number of optimum components is 4, Standard Error of Estimate (SEE) is 0.127.

Table 2. Statistical parameters of CoMFA and CoMSIA models for the training set based on the molecular docking.

Model	q^2	n	r^2	SEE	F	S%	E%	H%	D%	A%
CoMFA	0.798	4	0.980	0.127	304.977	34.9	65.1			
CoMSIA	0.848	4	0.992	0.08	769.202	8.7	29.2	16.6	24.6	20.9

q^2 is LOO cross-validated correlated coefficient, r^2 is non-cross-validated coefficient. n is the optimal number of components in the non-cross-validated coefficient analysis. SE is Standard Error of Estimate. F is the ratio of r^2 to $1.0 - r^2$. S% stands for contribution of steric field. E% stands for contribution of electrostatic field. H% stands for contribution of hydrophobic field. D% stands for contribution of hydrogen-bond donor field. A% stands for hydrogen-bond acceptor field.

In the CoMSIA model, the q^2 was as high as 0.848, r^2 was 0.992, with the number of components = 4 and SEE was 0.08. In the test set, the regression coefficients r^2 are 0.955, and 0.920, respectively, implying that the CoMFA and CoMSIA models were reliable and powerful in predicting pIC_{50} values. Table 3 shows the predicted pIC_{50} and residues between predicted and experimentally measured pIC_{50} values.

Table 3. Comparison of experimental activities (pIC₅₀ values), predicted activities (pIC₅₀ values) and residual values of all the 37 inhibitors were shown in the CoMFA and CoMSIA models.

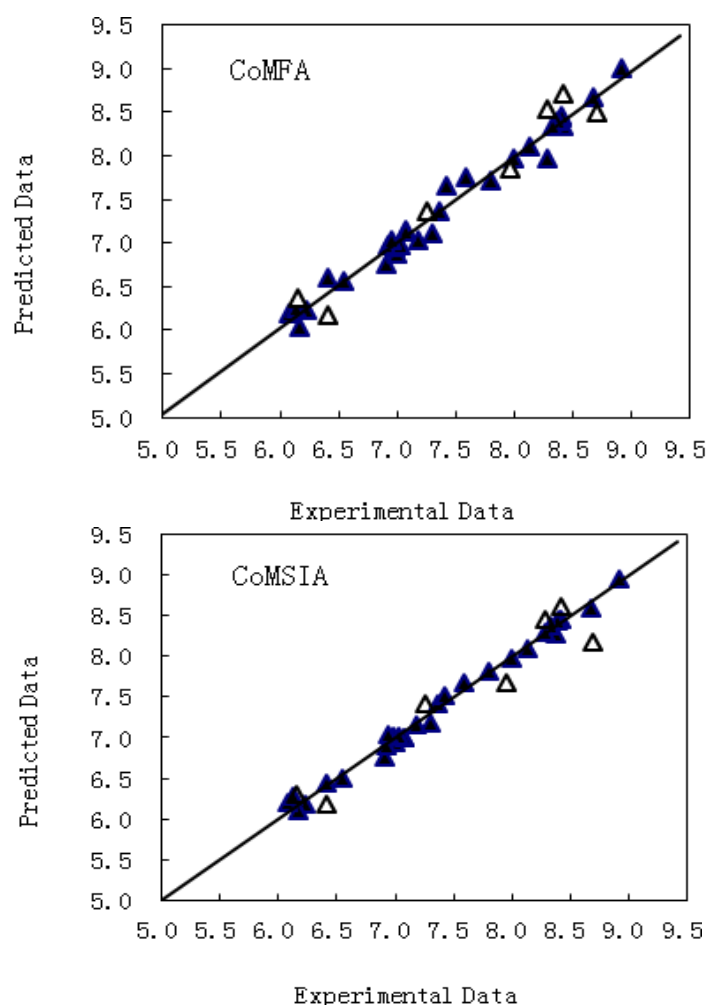
No.	Actual pIC ₅₀	CoMFA		CoMSIA	
		Predicted	Residues	Predicted	Residues
A ₀₁	8.9208	8.999	−0.0777	8.954	−0.0337
A ₀₂ *	8.699	8.495	0.2036	8.17	0.5294
A ₀₃	8.6778	8.679	−0.0015	8.587	0.0909
A ₀₄	8.4202	8.339	0.0816	8.459	−0.0387
A ₀₅ *	8.4202	8.708	−0.2881	8.603	−0.1826
A ₀₆	8.4089	8.445	−0.0361	8.443	−0.0342
A ₀₇	8.3979	8.448	−0.0499	8.424	−0.0263
A ₀₈	8.3768	8.399	−0.0218	8.268	0.109
A ₀₉	8.3279	8.334	−0.0058	8.377	−0.0494
A ₁₀ *	8.284	8.54	−0.2558	8.454	−0.1702
A ₁₁	7.9957	7.977	0.0185	7.977	0.0188
B ₀₁	7.585	7.747	−0.1617	7.685	−0.0997
B ₀₂ *	7.2596	7.372	−0.1129	7.408	−0.1481
B ₀₃	7.0706	7.148	−0.0774	7.009	0.0617
B ₀₄	6.9136	6.761	0.1527	6.768	0.1461
B ₀₅	7	6.884	0.1161	6.95	0.0499
B ₀₆	6.9872	6.95	0.0368	7.014	−0.0264
B ₀₇	6.9245	6.978	−0.0539	6.907	0.0174
B ₀₈ *	6.4078	6.183	0.2249	6.178	0.2301
B ₀₉	6.2328	6.232	0.0007	6.18	0.0533
B ₁₀	6.1637	6.031	0.1328	6.099	0.0648
B ₁₁	6.0814	6.201	−0.1191	6.207	−0.1256
B ₁₂	7.3565	7.362	−0.0054	7.42	−0.063
B ₁₃	7.1739	7.029	0.1451	7.165	0.0092
B ₁₄	6.5467	6.568	−0.0213	6.51	0.0362
B ₁₅	6.4089	6.597	−0.188	6.449	−0.0404
B ₁₆ *	6.1568	6.365	−0.2081	6.297	−0.1406
B ₁₇	6.1278	6.245	−0.1176	6.286	−0.1586
C ₀₁	8.284	7.976	0.308	8.293	−0.0092
C ₀₂	8.1308	8.108	0.0225	8.09	0.0411
C ₀₃ *	7.9586	7.85	0.1088	7.682	0.2764
C ₀₄	7.7959	7.71	0.0861	7.806	−0.0103
C ₀₅	7.4202	7.664	−0.2433	7.519	−0.0989
C ₀₆	7.301	7.119	0.1821	7.177	0.1243
C ₀₇	7.0757	7.135	−0.0597	7.008	0.0677
C ₀₈	7.0269	6.978	0.0491	7.01	0.0171
C ₀₉	6.9469	7.039	−0.0918	7.04	−0.0929

* Molecules belonging to the test set.

3.3. Predictive Power of 3D-QSAR Analyses

Figure 3 presents the prediction correlation of the CoMFA and CoMSIA models. Most of compounds were located on or near the trend line, implying the predicted pIC_{50} values are in good agreement with the experimental data, so the 3D-QSAR of both the CoMFA and CoMSIA models has good predictive value.

Figure 3. Correlation between the experimental and predicted values of the 3D-QSAR models for the training and test sets. The top figure is the CoMFA model; the bottom one is the CoMSIA model. The training set is shown by the filled triangles; the test set is shown by the empty triangles.



3.4. Graphical Interpretation of the Fields

The contour maps of different fields contribution of CoMFA and CoMSIA models are illustrated with inhibitor A_{01} as template (the compound with the highest inhibitive activity of all the Eg5 inhibitors). In the steric field contribution, green areas correspond to regions where steric occupancy with bulky polyhedral groups will increase affinity. Otherwise, yellow polyhedral areas should be sterically avoided. With the CoMSIA steric field map it is easier than with the CoMFA one to illustrate how steric effects affect the activity of inhibitors (Figures 4A,C). The pIC_{50} of A_{01} is 8.92 and that of

B_{11} is 6.08 so that we can analyze their steric field contour maps of the CoMSIA model to get more information about the effect of different groups on the activity. In Figure 4C, the difluorobenzene moiety of A_{01} is connected to a pyrazole ring with a nitrogen atom, while in B_{11} it is a carbon atom. Thus, their benzene rings have different spatial locations, the benzene ring's position in A_{01} is just located in the green region, but the benzene of ring B_{11} is in the yellow region of the steric field, while the R group of B_{11} is also in the yellow area and this reduces the activity. The electrostatic field maps of CoMFA and CoMSIA are shown in Figures 4B,D. Blue polyhedral regions represent an increase of positive charge that will enhance the binding affinity, while red polyhedral regions represent an increase of negative charge that will enhance affinity. In our results, the red areas in the CoMFA are less clear than in the CoMSIA study that displays some little red areas occupied by the ligands that will affect the right design for researchers.

Figure 4. Molecule A_{01} was placed inside of the fields of the CoMFA and CoMSIA models and all the contour cutoff levels were set at 80:20.

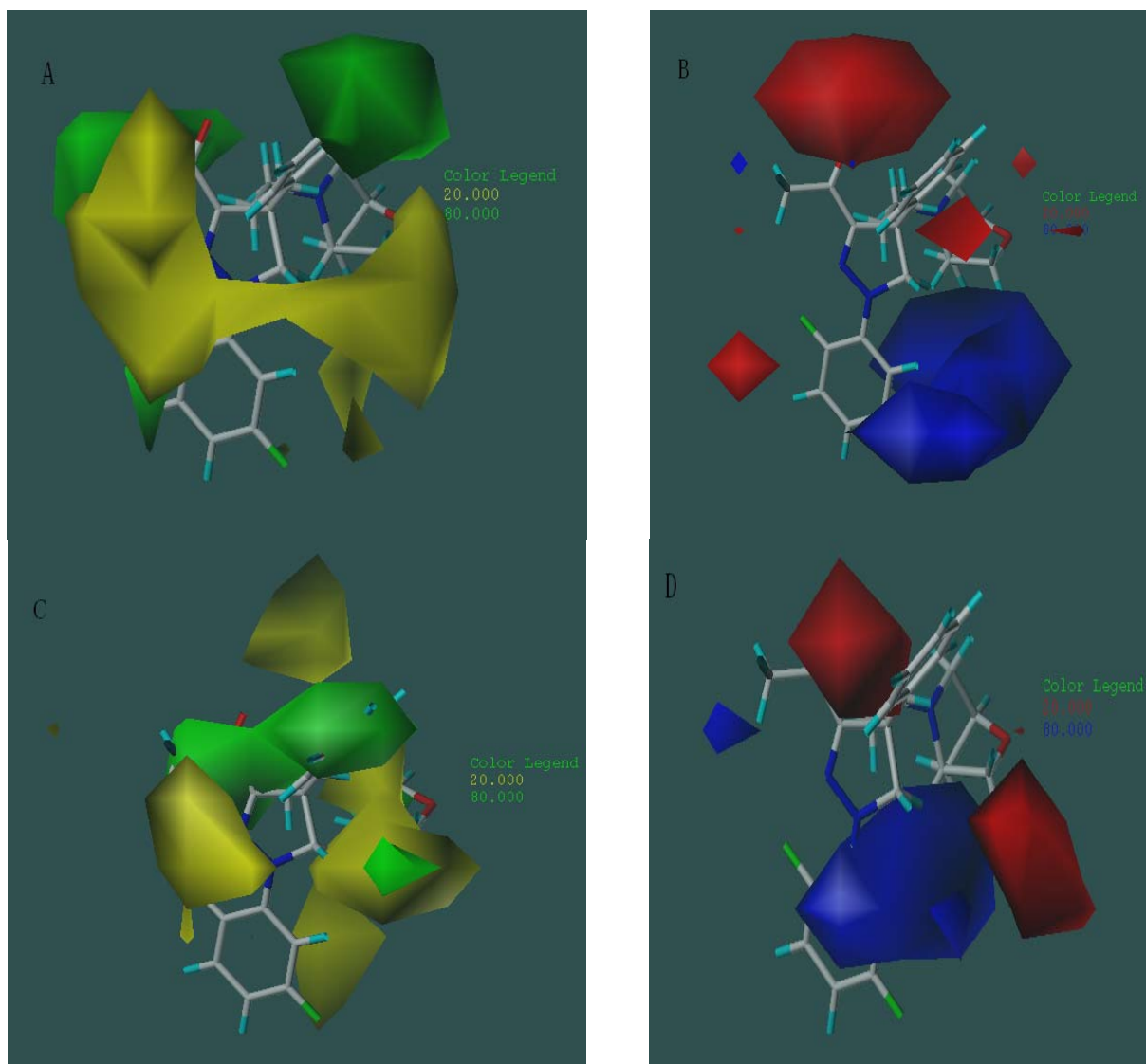
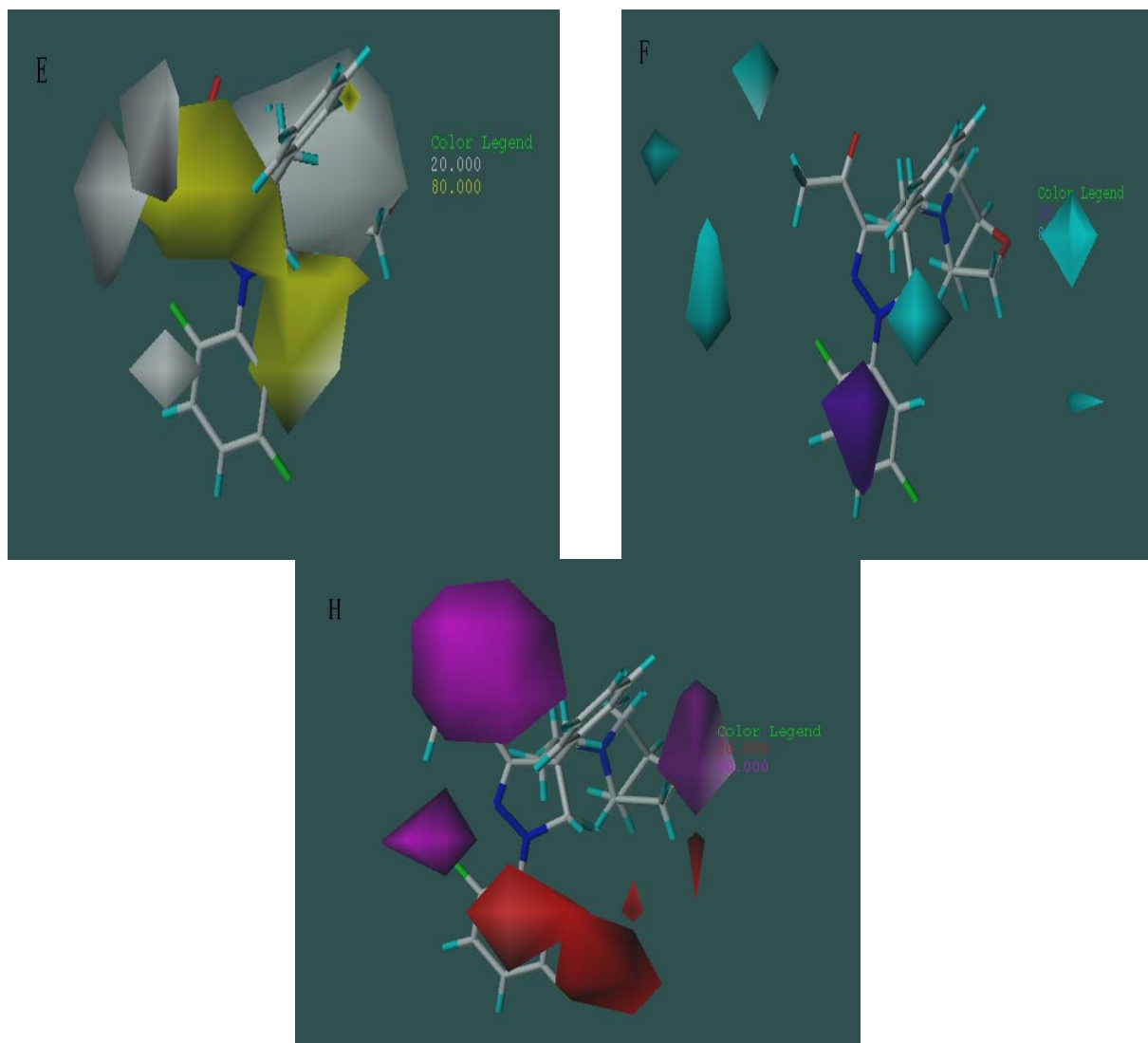


Figure 4. Cont.



(A) Steric field contour maps of the CoMFA model, where sterically favored areas were represented by green polyhedra; Sterically disfavored areas were represented by yellow polyhedra; (B) Electrostatic field contour maps of the CoMFA model, blue polyhedral regions represent an increase of positive charge that will enhance affinity; red polyhedral regions represent an increase of negative charge that will enhance affinity; (C) Steric field contour maps of the CoMSIA model, where green and yellow polyhedral regions represent favored and disfavored areas, respectively; (D) Electrostatic field contour maps of the CoMSIA model, where blue polyhedral regions represent an increase of positive charge that will enhance affinity; red polyhedral regions represent an increase of negative charge that will enhance affinity; (E) Hydrophobic field contour maps of the CoMSIA model, with hydrophobic favored areas represented by yellow polyhedra and hydrophobic disfavored areas represented by white polyhedra; (F) H-bond donor field contour maps of the CoMSIA model, where H-bond donor favored areas are represented by cyan polyhedral and H-bond donor disfavored areas are represented by purple polyhedra; (H) H-bond acceptor field contour maps of the CoMSIA model, with H-bond acceptor favored areas represented by magenta polyhedra and H-bond acceptor disfavored areas represented by red polyhedra.

The Figure 4D shows that the negative carboxyl of A₀₁ increased affinity in the red region, while B₁₁ does not have this effect. In the hydrophobic field contour maps of the CoMSIA model, hydrophobically favored areas were represented by yellow polyhedral and hydrophobically disfavored areas are represented by white polyhedra. Pyrazole rings are surrounded by the yellow polyhedra and also increase the hydrophobic affinity. A large white region on the R groups of A₀₁ indicated that hydrophilic properties were important for affinity (see Figure 4E). And high affinity and activity inhibitors would be designed under the analysis of the contour maps in different fields contribution.

In Figure 4F, in the H-bond donor field contour maps of the CoMSIA model, cyan polyhedra represent H-bond donor favored areas; while purple polyhedra represent the H-bond donor disfavored areas. The polyhedron areas in cyan near the pyrazole rings indicate that H on the position will increase binding affinity. The areas in purple near the difluorobenzene moiety of A₀₁ proved that the H on that position should decrease binding affinity and H bond acceptors or electron-rich groups should increase binding affinity.

In the H-bond acceptor field maps, H-bond acceptor favored areas are represented by magenta polyhedra while disfavored areas are represented by red polyhedra. In the Figure 4H, the heterocyclic carboxyl oxygen and the fluorine of A₀₁ encompassed by the large magenta areas show that a good H-bond acceptor, the difluorobenzene moiety of A₀₁, is surrounded by the red polyhedra, indicating that hydrogen in these areas on the ligands represents a low binding affinity.

4. Conclusions

Dihydropyrazole and dihydropyrrole derivatives have been described as novel and potent Eg5 inhibitors by Merck Research Laboratories [16–18]. These inhibitors have also been proven to have the potential to overcome the multidrug resistance of anticancer drugs, In this work, molecular docking and 3-D QSAR studies were carried out to explore the binding mechanism of dihydropyrazole and dihydropyrrole derivatives to EG5. Good prediction COMFA and COMSIA models were obtained with LOO cross-validation q^2 and conventional r^2 values of 0.898, 0.980, and 0.848, 0.992, respectively. The results show that ligands binding in the hydrophobic part of the inhibitor-binding pocket were found to be crucial for potent ligand binding and kinase selectivity. It is thus possible to gain insights into the relationship between the structural information of dihydropyrazole and dihydropyrrole inhibitors and their inhibitory potency, aimed at providing valuable guidance for the design of EG5 inhibitors with high anticancer activity.

Acknowledgments

This study was supported by the National Natural Science Foundation of China (60873103, 81171508, 31170747), New Drugs Creation national major projects (2009ZX09503-005), Key Project of Natural Science Foundation of China (No. 30830090), Natural Science Foundation project CQ CSTC (No. 2010BB5304), and Science and Technology project of Chongqing Education Commission (KJ110804).

References and Notes

1. Blangy, A.; Lane, H.A.; d'Herin, P.; Harper, M.; Kress, M.; Nigg, E.A. Phosphorylation by p34cdc2 regulates spindle association of human Eg5, a kinesin-related motor essential for bipolar spindle formation *in vivo*. *Cell* **1995**, *83*, 1159–1169.
2. Weil, D.; Garcon, L.; Harper, M.; Dumenil, D.; Dautry, F.; Kress, M. Targeting the kinesin Eg5 to monitor siRNA transfection in mammalian cells. *Biotechniques* **2002**, *33*, 1244–1248.
3. Mayer, T.U.; Kapoor, T.M.; Haggarty, S.J.; King, R.W.; Schreiber, S.L.; Mitchison, T.J. Small molecule inhibitor of mitotic spindle bipolarity identified in a phenotype-based screen. *Science* **1999**, *286*, 971–974.
4. Maliga, Z.; Kapoor, T.M.; Mitchison, T.J. Evidence that monastrol is an allosteric inhibitor of the mitotic kinesin Eg5. *Chem. Biol.* **2002**, *9*, 989–996.
5. Turner, J.; Anderson, R.; Guo, J.; Beraud, C.; Fletterick, R.; Sakowicz, R. Crystal structure of the mitotic spindle kinesin Eg5 reveals a novel conformation of the neck-linker. *J. Biol. Chem.* **2001**, *276*, 25496–25502.
6. DeBonis, S.; Skoufias, D.A.; Lebeau, L.; Lopez, R.; Robin, G.; Margolis, R.L.; Wade, R.H.; Kozielski, F. *In vitro* screening for inhibitors of the human mitotic kinesin Eg5 with antimetabolic and antitumor activities. *Mol. Cancer Ther.* **2004**, *3*, 1079–1090.
7. Skoufias, D.A.; DeBonis, S.; Saoudi, Y.; Lebeau, L.; Crevel, I.; Cross, R.; Wade, R.H.; Hackney, D.; Kozielski, F. S-trityl-L-cysteine is a reversible, tight binding inhibitor of the human kinesin Eg5 that specifically blocks mitotic progression. *J. Biol. Chem.* **2006**, *281*, 17559–17569.
8. Gartner, M.; Sunder-Plassmann, N.; Seiler, J.; Utz, M.; Vernos, I.; Surrey, T.; Giannis, A. Development and biological evaluation of potent and specific inhibitors of mitotic Kinesin Eg5. *ChemBioChem* **2005**, *6*, 1173–1177.
9. Kozielski, F.; DeBonis, S.; Skoufias, D.A. Screening for inhibitors of microtubule-associated motor proteins. *Methods Mol. Med.* **2007**, *137*, 189–207.
10. Orr, G.A.; Verdier-Pinard, P.; McDaid, H.; Horwitz, S.B. Mechanisms of Taxol resistance related to microtubules. *Oncogene* **2003**, *22*, 7280–7295.
11. Kavallaris, M. Microtubules and resistance to tubulin-binding agents. *Nat. Rev. Cancer* **2010**, *10*, 194–204.
12. Kaan, H.Y.; Weiss, J.; Menger, D.; Ulaganathan, V.; Tkocz, K.; Laggner, C.; Popowycz, F.; Joseph, B.; Kozielski, F. Structure-activity relationship and multidrug resistance study of new S-trityl-L-cysteine derivatives as inhibitors of Eg5. *J. Med. Chem.* **2011**, *54*, 1576–1586.
13. Barsanti, P.A.; Wang, W.; Ni, Z.-J.; Duhl, D.; Brammeier, N.; Martin, E.; Bussiere, D.; Walter, A.O. The discovery of tetrahydro- β -carboline as inhibitors of the kinesin Eg5. *Bioorg. Med. Chem. Lett.* **2010**, *20*, 157–160.
14. Liu, M.; Yu, H.; Huo, L.; Liu, J.; Li, M.; Zhou, J. Validating the mitotic kinesin Eg5 as a therapeutic target in pancreatic cancer cells and tumor xenografts using a specific inhibitor. *Biochem. Pharmacol.* **2008**, *76*, 169–178.
15. Xiao, S.; Shi, X.-X. The first highly stereoselective approach to the mitotic kinesin Eg5 inhibitor HR22C16 and its analogues. *Tetrahedron: Asymmetry* **2010**, *21*, 226–231.

16. Cox, C.D.; Torrent, M.; Breslin, M.J.; Mariano, B.J.; Whitman, D.B.; Coleman, P.J.; Buser, C.A.; Walsh, E.S.; Hamilton, K.; Schaber, M.D. Kinesin spindle protein (KSP) inhibitors. Part 4:1 Structure-based design of 5-alkylamino-3,5-diaryl-4,5-dihydropyrazoles as potent, water-soluble inhibitors of the mitotic kinesin KSP. *Bioorg. Med. Chem. Lett.* **2006**, *16*, 3175–3179.
17. Fraley, M.E.; Garbaccio, R.M.; Arrington, K.L.; Hoffman, W.F.; Tasber, E.S.; Coleman, P.J.; Buser, C.A.; Walsh, E.S.; Hamilton, K.; Fernandes, C. Kinesin spindle protein (KSP) inhibitors. Part 2: The design, synthesis, and characterization of 2,4-diaryl-2,5-dihydropyrrole inhibitors of the mitotic kinesin KSP. *Bioorg. Med. Chem. Lett.* **2006**, *16*, 1775–1779.
18. Roecker, A.J.; Coleman, P.J.; Mercer, S.P.; Schreier, J.D.; Buser, C.A.; Walsh, E.S.; Hamilton, K.; Lobell, R.B.; Tao, W.; Diehl, R.E. Kinesin spindle protein (KSP) inhibitors. Part 8: Design and synthesis of 1,4-diaryl-4,5-dihydropyrazoles as potent inhibitors of the mitotic kinesin KSP. *Bioorg. Med. Chem. Lett.* **2007**, *17*, 5677–5682.
19. Brier, S.; Lemaire, D.; Debonis, S.; Forest, E.; Kozielski, F. Identification of the protein binding region of S-trityl-L-cysteine, a new potent inhibitor of the mitotic kinesin Eg5. *Biochemistry* **2004**, *43*, 13072–13082.
20. Yi Kristal Kaan, H.; Ulaganathan, V.; Hackney, D.D.; Kozielski, F. An allosteric transition trapped in an intermediate state of a new kinesin-inhibitor complex. *Biochem. J.* **2010**, *425*, 55–60.
21. Debonis, S.; Skoufias, D.A.; Indorato, R.L.; Liger, F.; Marquet, B.; Laggner, C.; Joseph, B.; Kozielski, F. Structure-activity relationship of S-trityl-L-cysteine analogues as inhibitors of the human mitotic kinesin Eg5. *J. Med. Chem.* **2008**, *51*, 1115–1125.
22. Kozielski, F.; Skoufias, D.A.; Indorato, R.L.; Saoudi, Y.; Jungblut, P.R.; Hustoft, H.K.; Strozynski, M.; Thiede, B. Proteome analysis of apoptosis signaling by S-trityl-L-cysteine, a potent reversible inhibitor of human mitotic kinesin Eg5. *Proteomics* **2008**, *8*, 289–300.
23. Prokopcova, H.; Dallinger, D.; Uray, G.; Kaan, H.Y.; Ulaganathan, V.; Kozielski, F.; Laggner, C.; Kappe, C.O. Structure-activity relationships and molecular docking of novel dihydropyrimidine-based mitotic Eg5 inhibitors. *ChemMedChem* **2010**, *5*, 1760–1769.
24. Kubinyi, H. QSAR and 3D QSAR in drug design Part 1: Methodology. *Drug Discov. Today* **1997**, *2*, 457–467.
25. Cramer, R.D.; Patterson, D.E.; Bunce, J.D. Comparative molecular field analysis (CoMFA). 1. Effect of shape on binding of steroids to carrier proteins. *J. Am. Chem. Soc.* **1988**, *110*, 5959–5967.
26. Klebe, G.; Abraham, U.; Mietzner, T. Molecular similarity indices in a comparative analysis (CoMSIA) of drug molecules to correlate and predict their biological activity. *J. Med. Chem.* **1994**, *37*, 4130–4146.
27. Puntambekar, D.; Giridhar, R.; Yadav, M.R. 3D-QSAR studies of farnesyltransferase inhibitors: A comparative molecular field analysis approach. *Bioorg. Med. Chem. Lett.* **2006**, *16*, 1821–1827.
28. Zhang, H.; Liu, C.; Li, H. CoMFA and CoMSIA Studies of nAChRs Ligands: Epibatidine Analogues. *QSAR Comb. Sci.* **2004**, *23*, 80–88.
29. Zhang, Q.; Yu, C.; Min, J.; Wang, Y.; He, J.; Yu, Z. Rational questing for potential novel inhibitors of FabK from *Streptococcus pneumoniae* by combining FMO calculation, CoMFA 3D-QSAR modeling and virtual screening. *J. Mol. Model.* **2010**, *17*, 1483–1492.

30. AbdulHameed, M.D.; Hamza, A.; Liu, J.; Huang, X.; Zhan, C.G. Human microsomal prostaglandin E synthase-1 (mPGES-1) binding with inhibitors and the quantitative structure-activity correlation. *J. Chem. Inf. Model.* **2008**, *48*, 179–185.
31. Venkatachalam, C.M.; Jiang, X.; Oldfield, T.; Waldman, M. LigandFit: A novel method for the shape-directed rapid docking of ligands to protein active sites. *J. Mol. Graph. Model.* **2003**, *21*, 289–307.
32. Sippl, W. Application of Structure-Based Alignment Methods for 3D QSAR Analyses. In *Pharmacophores and Pharmacophore Searches*; Wiley-VCH Verlag GmbH & Co. KGaA: Weinheim, Germany, 2006; pp. 223–249.
33. Liu, T.; Lin, Y.; Wen, X.; Jorissen, R.N.; Gilson, M.K. BindingDB: A web-accessible database of experimentally determined protein-ligand binding affinities. *Nucleic Acids Res.* **2007**, *35*, D198–D201.

Sample Availability: Not available.

© 2012 by the authors; licensee MDPI, Basel, Switzerland. This article is an open access article distributed under the terms and conditions of the Creative Commons Attribution license (<http://creativecommons.org/licenses/by/3.0/>).